J Clin Periodontol 2016; 43: 180–192 doi: 10.1111/jcpe.12503

Journal of Clinical Periodontology

Rescuing failed oral implants via Wnt activation

Xing Yin[1,2,†], Jingtao Li[1,2,†], Tao Chen[1,2], Sylvain Mouraret[2], Girija Dhamdhere[2], John B. Brunski[2], Shujuan Zou[1] and Jill A. Helms[2]

[1]State Key Laboratory of Oral Diseases, West China Hospital of Stomatology, Sichuan University, Chengdu, China; [2]Division of Plastic and Reconstructive Surgery, Department of Surgery, Stanford School of Medicine, Stanford, CA, USA

Yin X, Li J, Chen T, Mouraret S, Dhamdhere G, Brunski JB, Zou S, Helms JA. Rescuing failed oral implants via Wnt activation. J Clin Periodontol 2016; 43: 180–192. doi: 10.1111/jcpe.12503

Abstract

Aim: Implant osseointegration is not always guaranteed and once fibrous encapsulation occurs clinicians have few options other than implant removal. Our goal was to test whether a WNT protein therapeutic could rescue such failed implants.

Material and Methods: Titanium implants were placed in over-sized murine oral osteotomies. A lack of primary stability was verified by mechanical testing. Interfacial strains were estimated by finite element modelling and histology coupled with histomorphometry confirmed the lack of peri-implant bone. After fibrous encapsulation was established peri-implant injections of a liposomal formulation of WNT3A protein (L-WNT3A) or liposomal PBS (L-PBS) were then initiated. Quantitative assays were employed to analyse the effects of L-WNT3A treatment.

Results: Implants in gap-type interfaces exhibited high interfacial strains and no primary stability. After verification of implant failure, L-WNT3A or L-PBS injections were initiated. L-WNT3A induced a rapid, significant increase in Wnt responsiveness in the peri-implant environment, cell proliferation and osteogenic protein expression. The amount of peri-implant bone and bone in contact with the implant were significantly higher in L-WNT3A cases.

Conclusions: These data demonstrate L-WNT3A can induce peri-implant bone formation even in cases where fibrous encapsulation predominates.

[†]Authors contributing equally to this work.

Key words: biomechanics; fibrosis; finite element analysis; osseointegration; osteogenesis

Accepted for publication 24 December 2015

A clinically successful implant exhibits direct contact between the implant surface and surrounding bone (Albrektsson et al. 1986). Conversely, a failed implant exhibits fibrous encapsulation, a condition where fibrous connective tissue layers form between the implant surface and bone (Rolfe et al. 2011). Precisely why peri-implant cells differentiate into fibroblasts *versus* osteoblasts is not entirely clear, but mechanical loading of an implant that lacks primary stability is clearly a contributing factor (Branemark et al. 1977, Adell et al. 1981, Albrektsson et al. 1981).

To better understand the variables influencing this fibroblast/osteoblast cell fate decision we developed a mouse model of successful oral implant osseointegration (Mouraret et al. 2014a) then modified the model to create a situation where implants would reliably fail (Mouraret et al. 2014b). This failure model was achieved by placing implants into over-sized osteotomies and, similar to what has been observed in large animal models (Soballe et al. 1992, Elmengaard et al. 2005, Barckman et al. 2013a, b, Jimbo et al. 2014) and humans (Adell et al. 1981). Murine implants with such gap-type interfaces develop persistent fibrous encapsulation and the implants fail (Mouraret et al. 2014b).

Fibrous encapsulation is a hallmark of failed implants (Tonetti & Schmid 1994), but it also occurs in response to a foreign body reaction (Coleman et al. 1974, Kastellorizios et al. 2015). A foreign body reaction is characterized by the infiltration of inflammatory cells, the presence of

Conflict of interest and source of funding statement

The authors declare no potential conflicts of interest with respect to the authorship and/or publication of this article.

This research project was supported by grants from National Institutes of Health (DE 024000) to J.B.B. and J.A.H. and National Natural Science Foundation of China (81500829) to J.L.

granulation tissue, the up-regulation of inflammatory markers, and the absence of osteogenic protein expression (Sela et al. 1986, Rolfe et al. 2011). In the murine implant failure model, however, inflammatory cell infiltration was minimal and osteogenic activity was prominent, at least at the edges of the osteotomy (Mouraret et al. 2014b). Cells in the fibrous tissue surrounding the implant were also actively proliferating (Mouraret et al. 2014b). These two attributes clearly distinguished the implant failure model from a foreign body reaction. Here, using this implant failure model, we tested the hypothesis that providing a biological therapeutic in the form of liposome-reconstituted WNT3A protein would be sufficient to induce peri-implant bone formation around implants that had already undergone fibrous encapsulation.

We first verified that implants placed in gap-type interfaces lacked primary stability using mechanical testing, finite element analyses and histology coupled with histomorphometry. Failed implant cases were then treated with either liposome-reconstituted human WNT3A protein (L-WNT3A) or control (liposomal PBS). A WNT stimulus was chosen because of the protein's well-characterized roles in bone formation and bone regeneration [reviewed in (Baron & Kneissel 2013, Yin et al. 2015, Hughes et al. 2006)]. Molecular, cellular, mechanical, mathematical/theoretical analyses were then employed to understand how this treatment affected the peri-implant response.

Material and Methods

Animals

All experimental protocols followed ARRIVE guidelines and were approved by the Stanford Committee on Animal Research. Every effort was taken to ensure the guiding principles of the three R's were followed. Wherever possible, we replaced the use of animals with quantitative in vitro assays and mathematical modelling. Careful design and analysis of the study supported a reduction in animals used and refinement was addressed by reducing suffering through the use of analgesics. CD1 wild-type, Axin2-$^{LacZ/+}$ and Axin2CreERT2$^{/+}$;R26R$^{mTmG/+}$ 3–5-month-old male mice were housed in a temperature-controlled environment with 12 h light/dark cycles and after implant placement were fed a soft food diet and water ad libitum. There was no evidence of infection or prolonged inflammation at any surgical sites.

Surgeries and implants

In total, 143 mice were used for the study; the genotypes and the numbers of implants inserted in each experiment group are presented in Tables S1–S3. For implant placement mice were anaesthetized with an intraperitoneal injection of Ketamine (80 mg/kg) and Xylazine (16 mg/kg). The mouth was rinsed using a povidone-iodine solution for 1 min. followed by a sulcular incision that extended from the maxillary first molar to the mid-point on the alveolar crest. A full-thickness flap was elevated. Osteotomies were created bilaterally on the maxillary edentulous ridges, 1.5 mm in front of the first maxillary molar, using a low-speed (800 rpm) dental engine. Titanium implants (0.62 mm diameter titanium-6 Aluminium-4 Vanadium alloy "Retopins"; NTI Kahla GmbH, Germany) were placed in the osteotomy. A small portion of the implant was left exposed, approximating the height of the gingiva. The surgical site was rinsed and then closed using non-absorbable single interrupted sutures (Ethicon monofilament 9-0; Johnson & Johnson Medical, New Brunswick, New Jersy, USA). Following surgery, mice received subcutaneous injections of buprenorphine (0.05–0.1 mg/kg) for analgesia once a day for 3 days. No evidence of infection or prolonged inflammation at surgical sites was detected.

Finite element analyses (FEA)

Implants were modelled in two configurations (Table S4): one in which the osteotomy diameter produced a tight-fit implant (control group) and one in which the osteotomy diameter resulted in a ~15 μm gap-type interface around the implant. Both conditions were modelled using FEA. Elastic moduli and Poisson's ratio for bone, implant, and fibrous tissue in the gap are provided in Table S5.

Dose–response assay of L-WNT3A

Bone graft material (BGM) was harvested from femurs and tibiae (Jing et al. 2015), and resembled that which is collected during bone graft harvesting in humans (Pape et al. 2010). In brief, the animal was killed, the tibiae and femurs were split longitudinally and the material in the exposed marrow cavity was collected by gentle scraping with a small dental tool. The collected BGM was pooled then divided into aliquots. In previous studies we ensured that BGM aliquots were equivalent in terms of cellular content, which was accomplished by measuring DNA content via a microplate fluorescence reader. Using this method the percent variation in DNA content was <20% (Jing et al. 2015). Each 20 μl aliquot was incubated in 150 μl of Dulbecco modified Eagle Medium (DMEM) with 10%FBS containing L-PBS or increasing concentrations of L-WNT3A. Treatment was carried out at 20°C for 1 h; afterwards BGM was transferred into 24-well plates and cultured in an additional 600 μl of DMEM at 37°C for 18 h after which RNA was isolated and reverse transcription was performed (Whyte et al. 2013). Quantitative RT-PCR was performed (Prism 7900HT Sequence Detection System and Power SYBR Green PCR Master Mix; Applied Biosystems, Thermo Fisher Scientific, Waltham, Massachusetts, USA). Levels of gene expression were determined by the $\Delta\Delta C_t$ method and normalized to GAPDH values. All reactions were performed in triplicate. Primers sequences for Axin2, Osterix and GAPDH were as described (Jing et al. 2015).

Preparation and delivery of L-WNT3A

Liposomal WNT3A (L-WNT3A) and L-PBS were prepared (Dhamdhere et al. 2014). A split-mouth design was employed and treatment groups are specified in Table S3. Mice being treated with L-PBS and L-WNT3A received injections beginning on post-implant day 7 (PID7). A 20 μl volume of L-WNT3A (total concentration = 0.56 ng/μl) or L-PBS was injected into the peri-implant environment using a Hamilton micro-syringe. Injections continued every 48 h until euthanasia.

Sample preparation and tissue processing

Mice were killed on PID7, 14 and 21. For those animals whose implants were subjected to mechanical testing, maxillae were harvested, the skin and outer layers of muscle were removed, and the tissues were fixed in ethanol, and then subjected to lateral stiffness testing (see below). For those animals whose implants were evaluated by histology/histomorphometry, tissues were fixed in the 4% paraformaldehyde overnight at 4°C. Samples were decalcified in 19% EDTA for 3 weeks and after complete demineralization, implants were gently removed from the samples. Specimens were then dehydrated through an ascending ethanol series prior to paraffin embedding. Eight-micron-thick longitudinal sections were cut and collected on Superfrost-plus slides (Mouraret et al. 2014b). Tissue sections prepared for histology, immunohistochemistry and immunofluorescence were prepared by one individual then quantified by a blinded individual.

Interfacial stiffness analyses

A stiffness test of implants in bone (see Table S1) was carried out as described in (Cha et al. 2015). Peri-implant samples were collected, processed and then de-identified and shipped for mechanical testing. The operator was blinded to the identity of the samples.

The test is based on measuring the lateral deflection of a cantilever beam whose end is embedded in a medium (i.e. bone). The deflection of the beam at the point of loading is given by the equation:

$$\delta = \frac{FL^3}{3EI}$$

F is load acting at a distance from where the beam protrudes from bone; E is Young's modulus; I is the moment of inertia of the beam and delta is the beam's deflection at its tip. To measure deflection maxillae containing implants were rigidly clamped to a solid support and positioned so that the implant was positioned between a stepper motor (Ultra Motion Digit, Mattituck, NY, USA) equipped with a 10N load transducer (Honeywell Model 31) and a displacement transducer (MG-DVRT-3, Lord MicroStrain, Williston, VT, USA). The test assumes that for very small forces (e.g. <1N) and deflections (e.g. <50 μm) the lateral deflection of the beam (implant) depends primarily on the properties of the interface. Accordingly, stiffness is represented by the term El, which is computed from the measured load-deflection data:

$$EI = \frac{FL^3}{3\delta}$$

Histology

Movat's pentachrome staining was performed. Nuclei stain blue to black, cytoplasm stains red, collagen stains yellow to greenish yellow, and fibrous tissue stains an intense red (Movat 1955). Aniline blue staining was used to detect osteoid matrix. Tissues were also stained with the acidic dye, picrosirius red, to discriminate tightly packed and aligned collagen molecules. Under polarized light, well-aligned fibrillary collagen molecules present polarization colours of longer wavelengths (red) as compared to less organized collagen fibrils that show colours of shorter wavelengths (green-yellow). (Lim et al. 2014).

Histomorphometry

Histomorphometric measurements were performed with IMAGEJ software 1.4 (NIH, Bethesda, Maryland, USA). Each implant resulted in a total of ~60 8-μm-thick sections; out of which a minimum of four sections were used for quantification. Images of the peri-implant environment were imported into IMAGEJ; a region of interest (ROI) was defined, and the total number of pixels within that ROI was determined. The pixels corresponding to new bone matrix within the same ROI were selected; the value was expressed as a percentage of the total ROI and labelled, %NBF.

A second histomorphometric analysis was performed, where the amount of bone in contact with the presumptive implant surface was calculated. Images corresponding to the presumptive area of bone-implant contact (BIC) were taken; images were imported into IMAGEJ and the total length of the interface between the tissue and the space once occupied by the implant was measured. The length of the interface that was occupied by bone was calculated within the same ROI, and expressed as %BIC.

Cellular assays

Alkaline phosphatase (ALP) activity was detected by incubation in nitro blue tetrazolium chloride (NBT; Roche), 5-bromo-4-chloro-3-indolyl phosphate (BCIP; Roche), and NTM buffer (100 mM NaCl, 100 mM Tris pH9.5, 5 mM MgCl).

Tartrate-resistant acid phosphatase (TRAP) activity was observed using a Leukocyte acid phosphatase staining kit (Sigma, St. Louis, Missouri, USA). After developing, the slides were dehydrated in a series of ethanol and xylene and subsequently cover-slipped with Permount mounting media.

For TUNEL staining, sections were incubated in proteinase K buffer (20 μg/ml in 10 mM Tris pH 7.5), applied to a TUNEL reaction mixture (In Situ Cell Death Detection Kit; Roche Indianapolis, Indiana, USA), and mounted with DAPI mounting medium (Vector Laboratories, Burlingame, California, USA). Slides were viewed under an epifluorescence microscope. The host response to L-WNT3A treatment was quantified by determining the number of dying cells in the peri-implant environment. The unit of analysis is the amount of TUNEL product produced by peri-implant cells.

For X-gal staining, $Axin2^{LacZ/+}$ tissues were fixed in 0.4% paraformaldehyde overnight before being decalcified with 19% EDTA and infused with 30% sucrose for 24 h. Samples were embedded in optimum cutting temperature (OCT) medium and cryosectioned at a thickness of 8 μm. Tissues were then fixed in 0.2% gluteraldehyde for 15 min. and stained with X-gal overnight at 37°C. The host response to L-WNT3A treatment was quantified by determining the number of cells that mounted a transcriptional response to the WNT stimulus in the peri-implant environment as described in (Popelut et al. 2010). The unit of analysis is the number of mRNA transcripts encoding the Wnt target gene, Axin2.

Immunohistochemistry and immunofluorescence

Tissue sections were deparaffinized following standard procedures. Endogenous peroxidase activity was quenched by 3% hydrogen peroxide for 5 min, and then washed in PBS. Slides were blocked with 5% goat serum (Vector S-1000) for 1 h at room temperature. The appropriate primary antibody was added and incubated overnight at 4°C, then washed in PBS. For immunohistochemistry, samples were incubated with appropriate biotinylated secondary antibodies (Vector BA-x) for 30 min. at room temperature, then washed in PBS. An advidin/biotinylated enzyme complex (Kit ABC Peroxidase Standard Vectastain PK-4000) was added and incubated for 30 min. and a DAB substrate kit (Vector Peroxidase substrate DAB SK-4100) was used to develop the colour reaction. For immunofluorescence, samples were incubated with fluorochrome-conjugated secondary antibody (1:500) for 30 min. at room temperature in the dark, and then mounted with DAPI mounting medium (Vector Laboratories). Slides were viewed under an epifluorescence microscope.

Primary antibodies and their dilutions were as follows: anti-Vimentin (1:100), anti-Ki67 (1:100), anti-PCNA (1:10,000), anti-Runx2 (1:200), anti-Osterix (1:500), anti-collagen type I (1:100), anti-Vimentin (1:100), anti-CD11b (1:200), anti-β-galactosidase (1:1000) and anti-biotinylated GFP (1:500). Each immunostaining reaction was accompanied by a negative control, where the primary antibody was not included. For all immunohistochemical reactions the host response to L-WNT3A treatment was quantified by determining the number of mitotically active/osteogenic/fibrogenic cells in the peri-implant environment; the unit of analysis was in cases the number of pixels corresponding to immunopositive cells.

Statistical analyses

Results are presented as the mean ± standard error values of independent replicates. One-way ANOVA was used in the dose–response assay of L-WNT3A and quantification of β-gal^{+ve} cells and GFP^{+ve} cells at multiple time points. Student's *t*-test was used in the interfacial stiffness analyses and quantification of peri-implant cellular activity after L-WNT3A/L-PBS treatment on PID14. Two-way ANOVA was used to quantify %NBF and %BIC at multiple time points. Significance was attained at $p < 0.05$ and all statistical analyses were performed with SPSS software (IBM, Armonk, New York, USA).

Results

A gap-type interface results in oral implant failure

Our primary objective was to test whether a WNT-based protein therapeutic was sufficient to reverse fibrous encapsulation of an implant. To test this hypothesis, we first created a mouse model of oral implant osseointegration (Mouraret et al. 2013) then modified it so as to create a reliable, reproducible model of fibrous encapsulation (Mouraret et al. 2014b). We began this study by characterizing the mechanical environment that contributed to the formation of this fibrous tissue envelope around oral implants.

Titanium implants were placed into the mouse maxillae, either into tight-fit osteotomies or over-sized osteotomies created on the edentulous ridge (Figs 1A,B and S1). A small portion of the implant was left exposed, approximating the height of the gingiva (Fig. 1C). Immediately after placement, mechanical testing was used to measure lateral stability (Fig. 1D). Relative to tight-fit implants ($N = 5$), gap-type implants ($N = 5$) exhibited lateral instability. For example a lateral force of 0.6N was required to cause a 40 μm displacement of tight-fit implants, whereas a lateral load of only 0.02N was required to displace the gap-type implants the same distance (Fig. 1E). Therefore, the interface around tight-fit implants was significantly stiffer than the elastic and deformable interface around gap-type implants.

We evaluated the consequences of a stiff *versus* elastic interface using FEA. Histology guided the formulation of geometries used in the FE models, where the implant was modelled as a solid screw positioned in either an oversized or a tight-fit osteotomy created in a cylinder of bone. To simulate a minimal level of masticatory force as would be experienced by implants placed at the level of the gingiva, an axial and lateral force = 0.01N was applied (Fig. 1F). In tight-fit implants the resulting distributions of compressive and tensile strains in the peri-implant bone were low (i.e. 0.0012% and +0.00088%, respectively, Fig. S1J), whereas around gap-type implants compressive and tensile strains were very high, on the order of 100% or greater, and concentrated at the crests of the threads (Fig. 1G).

The tissue response to such high interfacial strains was evaluated using histology and histomorphometric analyses at multiple time points after implant placement. Compared to control tight-fit implants ($N = 12$), implants in a gap-type interfaces had only fibrous tissue in contact with implant ($N = 12$; Fig. 1H).

Additional histology-based criteria were used to assess implant failure. For example compared to tight-fit implants (Fig. S1) gap-type implants were surrounded on post-implant day (PID) 7 by an inflammatory infiltrate (Fig. 1I,J). The fibrous tissue lacked collagen, as shown by picrosirius red staining (Fig. 1K). The inflammatory response resolved by PID14 (Fig. 1L) but the fibrous envelope persisted around gap-type implants (Fig. 1M,N). Even at the later stages of the study (PID21) minimal collagen was detectable around the implants (Fig. 1O–Q). From these in vivo, quantitative assays and mathematical modelling we conclude that implants placed into over-sized osteotomies exhibit poor stability, which leads to high interfacial strains in the peri-implant environment, and persistent fibrous encapsulation.

Fibrosis represents an end stage of healing around gap-type implants

Histology and immunohistochemistry were used to understand the fate of the fibrous tissue around gap-type implants. TUNEL staining for apoptotic cells revealed that the majority of dying cells in the peri-implant space were localized to what would have been the area of implant contact (Fig. 2A). By PID14, additional TUNEL^{+ve} cells were

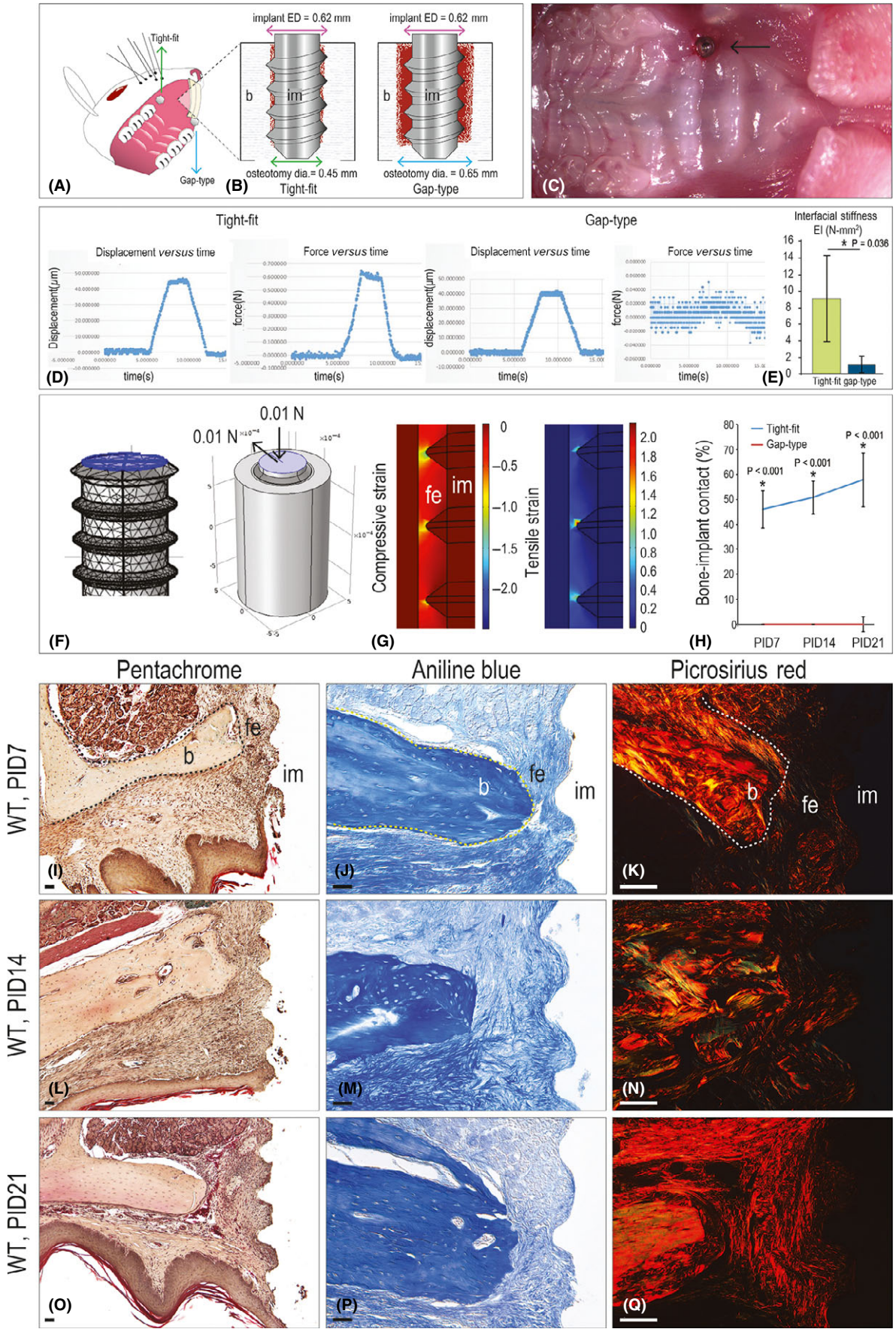

Fig. 1. A model of fibrous encapsulation and implant failure. (A) Schematic of the implant insertion site in the mouse oral cavity and (B) of the tight-fit and gap-type interfaces. (C) Intra-oral photograph of the implant, immediately after placement. (D) Representative displacement (μm) *versus* time (sec), and force (N) *versus* time (s), collected from tight-fit and gap-type implants. (E) Interfacial stiffness (represented by EI values) of tight-fit and gap-type interfaces. (F) Three-dimensional finite element model of gap-type implants. (G) Principal compressive strain and principal tensile strain in the gap-type interface. (H) Quantification of %BIC in tight-fit (blue) and gap-type (red) implants at the time points indicated. (I) Representative sagittal tissue sections from implants with gap-type interfaces analysed on PID7 ($N = 12$), (L) 14 ($N = 12$) and (O) 21 ($N = 12$). (J) Representative sagittal tissue sections stained with aniline blue to detect osteoid matrix on PID7 ($N = 12$), (M) 14 ($N = 12$) and (P) 21 ($N = 12$). (K) Representative sagittal tissue sections stained with picrosirius red to detect collagen organization on PID7 ($N = 12$), (N) 14 ($N = 12$) and (Q) 21 ($N = 12$). Abbreviations: BIC, bone-implant contact; b, bone; dia, diameter; ED, external diameter; fe, fibrous envelope; im, implant; PID, post-implant day; WT, wild-type. Scale bar = 50 μm for all panels.

distributed throughout the gap interface (Fig. 2B). By PID21, only a few apoptotic cells remained (Fig. 2C). Vimentin was used as a molecular marker of fibrosis (Akhmetshina et al. 2012) and immunostaining clearly showed that the persistence of fibrotic tissue throughout the entire examination period (Fig. 2D–F). Concurrent with this fibrosis, cells in the gap continued to proliferate as indicated by the presence of Ki67^{+ve} immunostaining (Fig. 2G–I).

Fibrous encapsulation of a failed dental implant has been likened to a foreign body reaction. To determine if the fibrous tissue around the implants was actually constituted a foreign body reaction, expression levels of inflammatory and osteogenic markers were evaluated. On PID7 the transcription factor Osterix (Nakashima et al. 2002) was expressed at high levels in the peri-implant space (Fig. 2J); other osteogenic proteins were initially high but diminished over the course (Figs 2K, L and S2). The monocyte/macrophage marker CD11b (Chen et al. 1993) was expressed at relatively high levels initially (Fig. 2M), commensurate with previous histological observations (Fig. 1), but as with the osteogenic markers, expression did not persist (Fig. 2N,O).

Wnt responsive cells are present in the fibrous tissue envelope

Within the fibrous connective tissue envelope around failed implants a

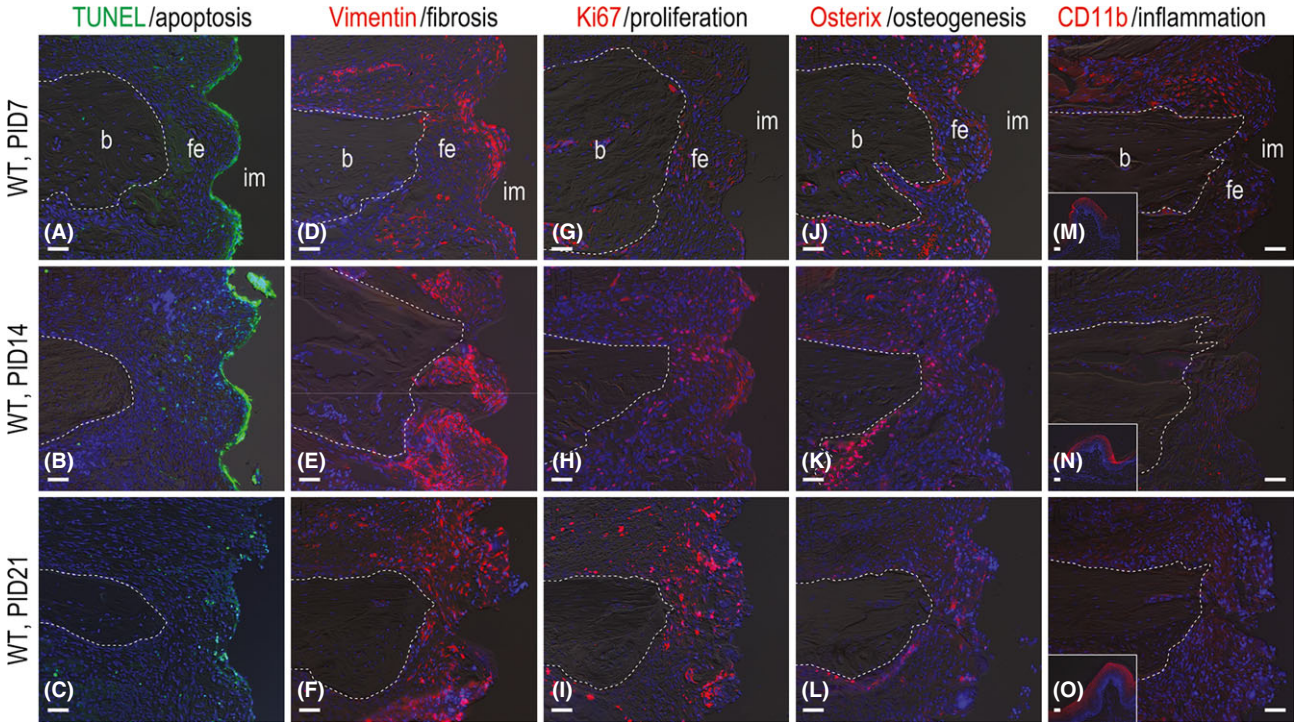

Fig. 2. Fibrous encapsulation of gap-type implants is terminal. (A) Representative sagittal tissue sections stained to detect cell nuclei (DAPI, blue) and cells undergoing apoptosis (TUNEL, green) on PID7 ($N = 12$), (B) 14 ($N = 12$) and (C) 21 ($N = 12$). (D) Immunostaining with Vimentin to detect fibroblasts on PID7 ($N = 12$), (E) 14 ($N = 12$) and (F) 21 ($N = 12$). (G) Immunostaining with Ki67 to detect cell proliferation on PID7 ($N = 12$), (H) 14 ($N = 12$), and (I) 21 ($N = 12$). (J) Immunostaining with Osterix to detect pre-osteoblasts on PID7 ($N = 12$), (K) 14 ($N = 12$) and (L) 21 ($N = 12$). (M) Immunostaining with CD11b to detect monocyte/macrophage on PID7 ($N = 12$), (N) 14 ($N = 12$) and (O) 21 ($N = 12$). Abbreviations: b, bone; CD11b, cluster of differentiation molecule 11b; fe, fibrous envelope; im, implant; PID, post-implant day; TUNEL, terminal deoxynucleotidyl Transferase-mediated dUTP nick end labelling; WT, wild-type. Scale bar = 50 μm for all panels.

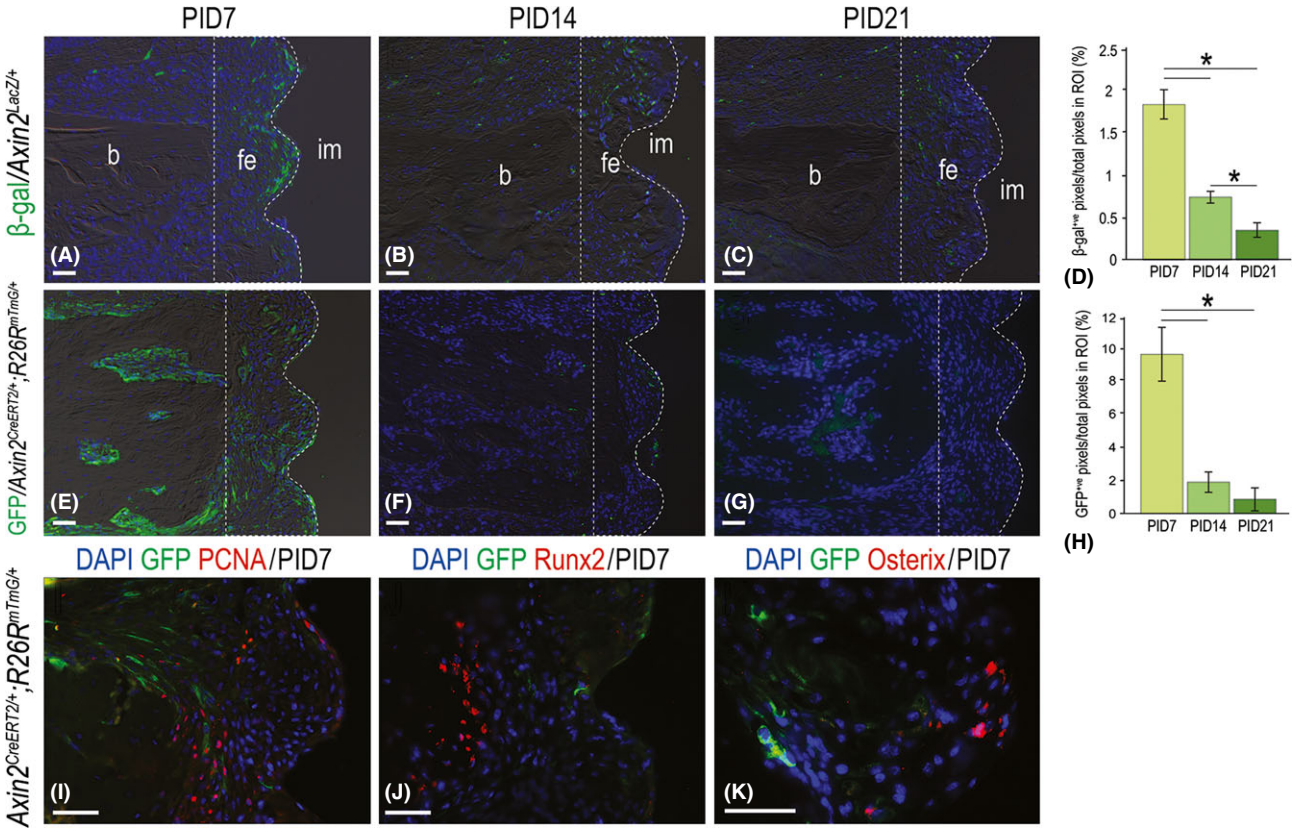

Fig. 3. A subset of Wnt responding cells in the peri-implant environment diminished with time. (A) Representative sagittal $Axin2^{LacZ/+}$ tissue sections immunostained with β-gal to detect Wnt responsive cells on post-implant day 7 ($N = 12$), (B) 14 ($N = 12$) and (C) 21 ($N = 12$), quantified in (D). (E) Representative sagittal tissue sections from $Axin2^{CreERT2/+}$;$R26R^{mTmG/+}$ mice, immunostained with GFP to detect Wnt responsive cells on post-implant day 7 ($N = 12$), (F) 14 ($N = 12$) and (G) 21 ($N = 12$), quantified in (H). (I) Representative sagittal tissue sections from $Axin2^{CreERT2/+}$;$R26R^{mTmG/+}$ mice, co-immunostained with GFP and PCNA, (J) Runx2 and (K) Osterix on PID7. Abbreviations: β-gal, β-galactosidase; b, bone; fe, fibrous envelope; im, implant; PID, post-implant day; ROI, region of interest. Scale bar = 50 μm for all panels.

population of Wnt responsive cells was identified. This was accomplished using the Wnt reporter strain, $Axin2^{LacZ/+}$ and β-galactosidase staining, which identified Wnt responsive cells in the gap interface (Fig. 3A). The density of Wnt responsive cells in the peri-implant environment diminished over time (Fig. 3B,C; quantified in D). To understand the basis for this decrease in Wnt responsive cells a second Wnt reporter strain $Axin2^{CreERT2/+}$;$R26R^{mTmG/+}$ (van Amerongen et al. 2012) was used. In the $Axin2^{CreERT2/+}$;$R26R^{mTmG/+}$ strain the GFP marker is transmitted to the cell's progeny and thus acts as a lineage tracer (Kretzschmar & Watt 2012). Tamoxifen was delivered to mice at the time of implant placement to induce recombination.

As observed previously, the number of Wnt responsive GFP^{+ve} cells diminished over time (Fig. 3E–G; quantified in H). Co-immunostaining with GFP and the cell proliferation marker PCNA revealed very few double-positive cells (Fig. 3I). Likewise, co-immunostaining with GFP and pre-osteoblast markers Runx2 and Osterix also failed to identify any double-labelled cells (Fig. 3J,K).

Fig. 4. L-WNT3A activates osteogenesis in the peri-implant environment. (A) Quantitative reverse transcription polymerase chain reaction for Axin2 in BGM in response to L-PBS and increasing concentrations of L-WNT3A ($N = 5$ for each condition). (B) Same conditions as in A, measuring the fold change in Osterix ($N = 5$). (C) On PID14, representative sagittal $Axin2^{LacZ/+}$ tissue sections stained with X-gal to detect Wnt responsive cells after L-PBS ($N = 6$) and (D) L-WNT3A ($N = 6$) injections, quantified in (E). (F) Immunostaining with β-gal to detect Wnt responsive cells after L-PBS ($N = 6$) and (G) L-WNT3A ($N = 6$) injections, quantified in (H). (I) Tissue sections stained to detect cell nuclei (DAPI, blue) and cells undergoing apoptosis (TUNEL, green) following L-PBS ($N = 12$) and (J) L-WNT3A ($N = 12$) injections, quantified in (K). (L) Immunostaining with PCNA to detect proliferation following L-PBS ($N = 12$) and (M) L-WNT3A ($N = 12$) injections, quantified in (N). (O) Fluorescence immunostaining for Osterix following L-PBS ($N = 12$) and (P) L-WNT3A ($N = 12$). (Q) Osterix immunostaining following L-PBS ($N = 12$) and (R) L-WNT3A ($N = 12$), quantified in (S). Abbreviations: b, bone; BGM, bone graft material; fe, fibrous envelope; im, implant; PID, post-implant day; WT, wild-type. Scale bar = 50 μm for all panels.

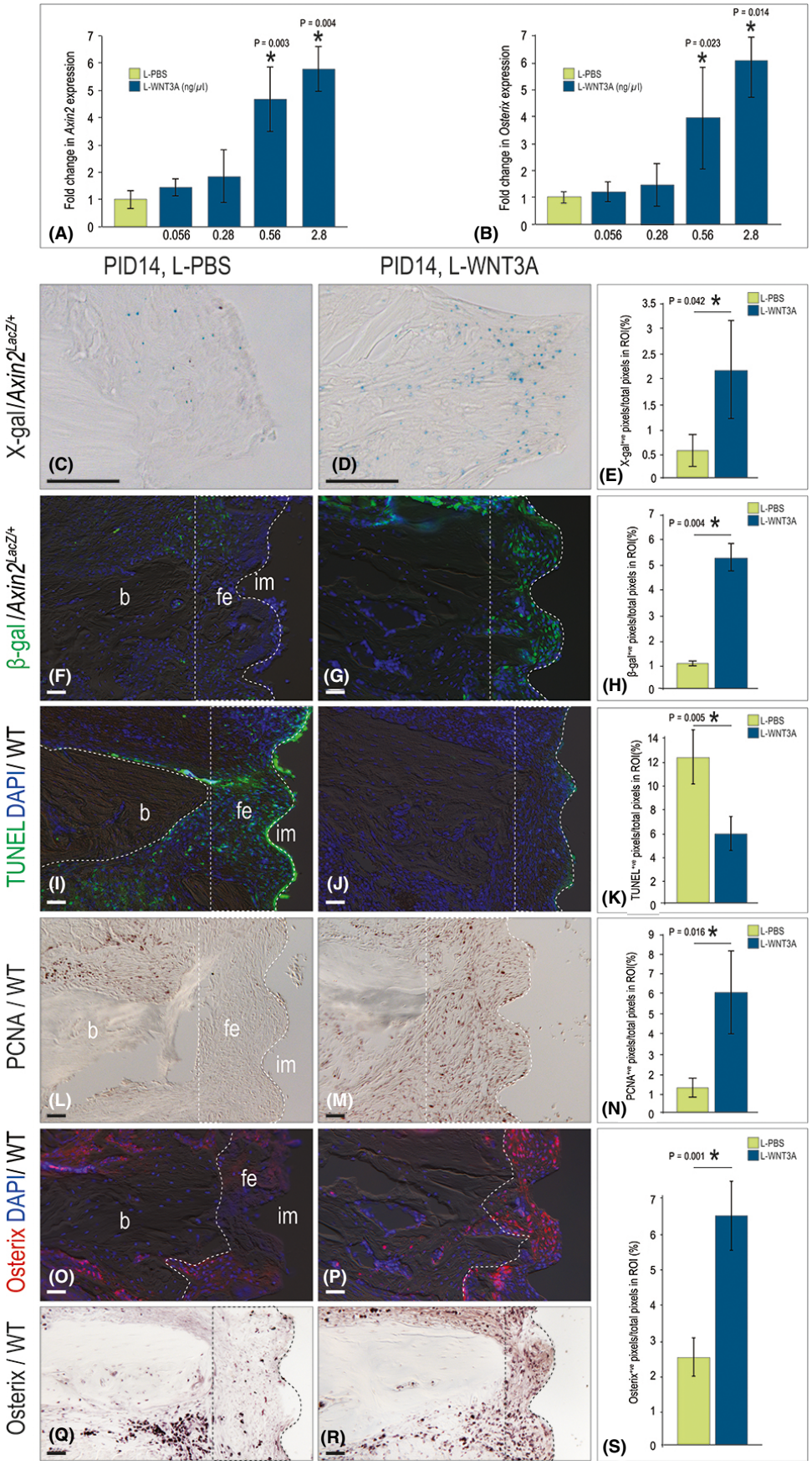

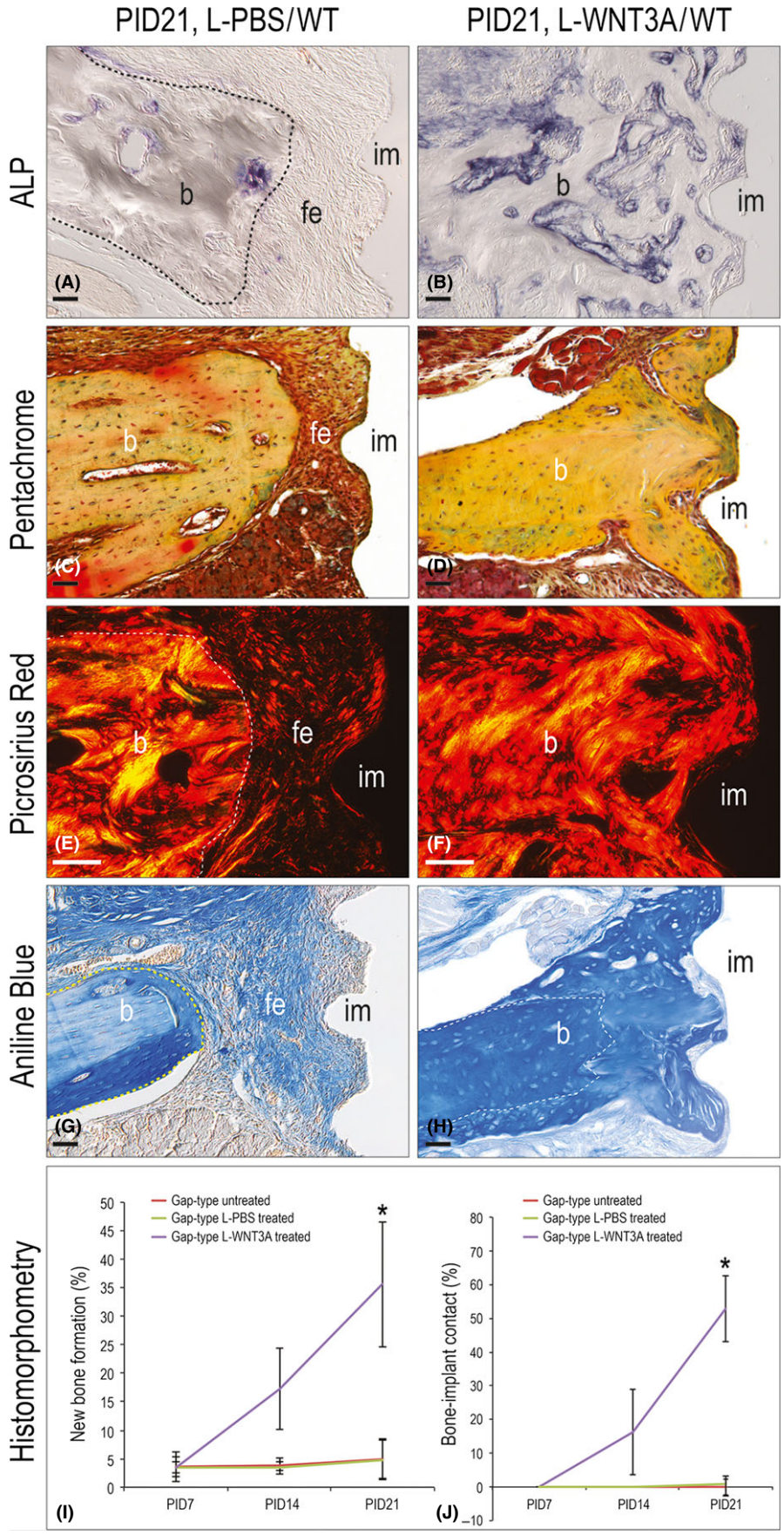

Thus, Wnt responsive cells and their progeny initially exist in the fibrous connective tissue envelope surrounding a failed implant but this cell population is lost over time through programmed cell death.

Exogenous Wnt signal stimulates osteogenic activity within the peri-implant environment

Genetically increasing Wnt signalling around an implant improved osseointegration (Mouraret et al. 2014b). Consequently, we reasoned that delivery of a Wnt protein therapeutic might be sufficient to induce bone formation in the gap interface. Based on dose–response data (Fig. 4A,B) 0.56 ng/μl L-WNT3A was used. Since pathway activation lasts for ~48 h in vivo (Dhamdhere et al. 2014), a 2-day interval was chosen. A split-mouth design was used and peri-implant injections of L-WNT3A and L-PBS began on PID7 when fibrous encapsulation is established (Fig. 1). Analyses were carried out on PID14.

L-WNT3A treatment elicited a strong Wnt response by cells in the peri-implant environment (Fig. 4C, D,F,G; quantified in E,H). This burst in Wnt signalling was accompanied by a significant drop with apoptosis (Fig. 4I,J; quantified in K) and a significant burst in proliferation in the peri-implant environment (Fig. 4L,M; quantified in N). In those implant cases treated with L-WNT3A, Osterix expression levels were significantly higher (Fig. 4O,P; quantified in S). The distribution of Osterix^{+ve} cells was also different: in L-PBS-treated cases, Osterix^{+ve} cells were located adjacent to the periosteal surfaces (Fig. 4Q); whereas in L-WNT3A-treated cases, Osterix^{+ve} cells were found throughout the fibrous tissue envelope (Fig. 4R). Together, these data demonstrated that L-WNT3A treatment reduced cell death, enhanced cell proliferation, and the initiation of osteogenesis in the peri-implant environment.

Fibrous encapsulation of an implant is reversed by L-WNT3A

On PID21, after 2 weeks of L-WNT3A or L-PBS peri-implant injections, robust ALP activity was evident around L-WNT3A-treated implants (Fig. 5A,B). Control, L-PBS-treated implants continued to exhibit fibrous encapsulation, whereas L-WNT3A-treated implants exhibited robust new bone formation (Fig. 5C,D). Well-organized collagen-rich mineralized matrix was in evidence around L-WNT3A-treated implants (Fig. 5E,F). Aniline blue histology showed the generation of osteoid matrix in the place where the fibrous encapsulation had existed (Fig. 5G,H).

Histomorphometric analyses on PID21 demonstrated that only 16% (2/12) of gap-type implants treated with L-PBS showed evidence of peri-implant bone formation, whereas 100% (12/12) of implants treated with L-WNT3A did (Fig. 5I). We also evaluated bone formation in contact with what would have been the implant surface: None of PBS-treated gap-type implants (12/12) showed evidence of bone in contact with the implant surface, whereas 84% (10/12) of L-WNT3A-treated implants had bone in contact with the implant (Fig. 5J). Bone remodelling was also evaluated and unlike bisphosphonates (Pazianas & Abrahamsen 2011), L-WNT3A treatment did not inhibit bone remodelling (TRAP staining, Fig. S3). We conclude that L-WNT3A stimulated bone formation around implants that had undergone fibrous encapsulation.

Discussion

Whether it is intended to replace a tooth, serve as an anchor, or substitute for a joint, implants must undergo osseointegration to be functional. Although it is not a guarantee, implants that exhibit primary stability at the time of placement typically osseointegrate (Javed & Romanos 2010) and certainly do so more reliably than implants lacking primary stability (Lioubavina-Hack et al. 2006). Consequently, clinicians strive to place implants that exhibit primary stability (O'Sullivan et al. 2004).

The fibrous capsule that forms around failed implants bears some similarity to a foreign body reaction (Anderson et al. 2008) but there is one critical difference: foreign body reactions are accompanied by chronic inflammation, whereas not all fibrous envelopes that surround failed implants share this feature ((Esposito et al. 2000) and see Fig. 2). This lack of chronic inflammation is an important distinction because it suggests that the non-inflamed tissue still has the ability to mount a repair or regenerative response.

In the past decade, an abundant literature has confirmed that elevating Wnt signalling promotes bone formation. For example increasing Wnt signalling through inhibition of the Wnt antagonists Dkk1 or Sclerostin are effective methods to induce bone formation in pathological conditions such as multiple myeloma (Yaccoby et al. 2007, Fulciniti et al. 2009) and osteoporosis (Canalis 2013, Recker et al. 2015). Recently, investigators have verified that the same anti-Sclerostin antibodies can increase bone formation around implants placed in the medullary cavities of long bones (Virdi et al. 2015).

In our own studies, we opted to make use of the WNT protein itself (Morrell et al. 2008, Zhao et al. 2009, Dhamdhere et al. 2014). Therapeutic proteins offer distinct advantages over small molecules and antibodies because of their specificity

Fig. 5. L-WNT3A reverses peri-implant fibrous encapsulation. (A) Representative sagittal tissue sections stained with ALP to detect mineralized activity after 14 days of L-PBS (N = 12) and (B) L-WNT3A (N = 12) injections. (C) Tissue sections stained with Movat's pentachrome after 14 days of L-PBS (N = 12) and (D) L-WNT3A (N = 12) injections. (E) Tissues stained with picrosirius red after 14 days of L-PBS (N = 12) and (F) L-WNT3A (N = 12) injections. (G) Aniline blue staining to detect new osteoid matrix after 14 days of L-PBS (N = 12) and (H) L-WNT3A (N = 12) injection. (I) Quantification of peri-implant new bone formation (% NBF) at time points indicated. (J) Quantification of bone-implant contact (%BIC) at time points indicated. Abbreviations: BIC, bone-implant contact; b, bone; fe, fibrous envelope; im, implant; NBF, new bone formation; PID, post-implant day; WT, wild-type. Scale bar = 50 μm for all panels.

and potency (Smith 2015). In other types of skeletal applications, L-WNT3A has the ability to induce bone healing in fractures, in spinal fusions, and in segmental bone defects (Minear et al. 2010, Leucht et al. 2013, Jing et al. 2015). In all these scenarios, however, the protein therapeutic was delivered within hours of the injury; here, we tested the ability of L-WNT3A to reverse a chronic state of fibrosis. Also, previous studies were carried out in the appendicular and axial skeleton, whereas this study specifically focused on craniofacial alveolar bone, and numerous studies including those from our group have identified genetic, molecular, and cellular differences in the healing responses of these bones (Leucht et al. 2008).

There are limitations to this study. Peri-implant injections were sufficient to up-regulate Wnt pathway activity in cells of the peri-implant environment (Fig. 4) and induce peri-implant bone formation (Fig. 5), but neither the method of delivery nor the dosing regimens were optimized. Future studies in larger rodents will address these important clinical variables. Also, decalcified tissue sections were used and although great care was taken to preserve the peri-implant tissues we nonetheless had to limit our conclusions to peri-implant osteogenesis and avoid conclusions about osseointegration. In these experiments, we purposefully created a situation where implants lacked primary stability, and thus would reliably fail (Fig. 1). This situation allowed us to evaluate the potential therapeutic value of L-WNT3A for treatment of implants that had undergone fibrous encapsulation (Figs 4 and 5). These data demonstrate that peri-implant bone formation can be induced, even in cases where fibrous encapsulation is established.

Clinicians strive to achieve implant stability at the time of insertion (Grandi et al. 2013) but for a variety of reasons, this can be challenging to attain. When implants lack primary stability, clinicians have few treatment choices. Sometimes the implant is submerged to prevent loading, with the hope that given sufficient time osseointegration will occur (Cecchinato et al. 2004). This submersion protocol presumes that loading was the primary cause of implant failure, and that once the implant is free from loading it will osseointegrate, but there is scant data to support this supposition. If this strategy is unsuccessful then the implant must be removed and replaced.

Conclusion

The feasibility of a WNT-based protein therapeutic to stimulate peri-implant bone formation was demonstrated in a mouse model of oral implant failure. Such a biological approach, if validated, would represent a significant addition to the clinicians' armamentarium for salvaging implants that have undergone fibrous encapsulation.

Acknowledgements

We thank A. Matthews, E. Zhang and D. Mitchell who contributed to this work.

References

Adell, R., Lekholm, U., Rockler, B. & Branemark, P. I. (1981) A 15-year study of osseointegrated implants in the treatment of the edentulous jaw. *International Journal of Oral Surgery* **10**, 387–416.

Akhmetshina, A., Palumbo, K., Dees, C., Bergmann, C., Venalis, P., Zerr, P., Horn, A., Kireva, T., Beyer, C., Zwerina, J., Schneider, H., Sadowski, A., Riener, M. O., MacDougald, O. A., Distler, O., Schett, G. & Distler, J. H. (2012) Activation of canonical Wnt signalling is required for TGF-beta-mediated fibrosis. *Nature Communications* **3**, 735. doi:10.1038/ncomms1734.

Albrektsson, T., Branemark, P. I., Hansson, H. A. & Lindstrom, J. (1981) Osseointegrated titanium implants. Requirements for ensuring a long-lasting, direct bone-to-implant anchorage in man. *Acta Orthopaedica Scandinavica* **52**, 155–170.

Albrektsson, T., Jansson, T. & Lekholm, U. (1986) Osseointegrated dental implants. *Dental Clinics of North America* **30**, 151–174.

van Amerongen, R., Bowman, A. N. & Nusse, R. (2012) Developmental stage and time dictate the fate of Wnt/beta-catenin-responsive stem cells in the mammary gland. *Cell Stem Cell* **11**, 387–400. doi:10.1016/j.stem.2012.05.023.

Anderson, J. M., Rodriguez, A. & Chang, D. T. (2008) Foreign body reaction to biomaterials. *Seminars in Immunology* **20**, 86–100. doi:10.1016/j.smim.2007.11.004.

Barckman, J., Baas, J., Sorensen, M., Bechtold, J. E. & Soballe, K. (2013a) Rinsing of allograft bone does not improve implant fixation: a study in 12 dogs. *Acta Orthopaedica* **84**, 307–313. doi:10.3109/17453674.2013.797314.

Barckman, J., Baas, J., Sorensen, M., Bechtold, J. E. & Soballe, K. (2013b) Periosteal augmentation of allograft bone and its effect on implant fixation - an experimental study on 12 dogs(). *The Open Orthopaedics Journal* **7**, 18–24. doi:10.2174/1874325001307010018.

Baron, R. & Kneissel, M. (2013) WNT signaling in bone homeostasis and disease: from human mutations to treatments. *Nature Medicine* **19**, 179–192. doi:10.1038/nm.3074.

Branemark, P. I., Hansson, B. O., Adell, R., Breine, U., Lindstrom, J., Hallen, O. & Ohman, A. (1977) Osseointegrated implants in the treatment of the edentulous jaw. Experience from a 10-year period. *Scandinavian Journal of Plastic and Reconstructive Surgery* 16, 1–132.

Canalis, E. (2013) Wnt signalling in osteoporosis: mechanisms and novel therapeutic approaches. *Nature Reviews. Endocrinology* **9**, 575–583. doi:10.1038/nrendo.2013.154.

Cecchinato, D., Olsson, C. & Lindhe, J. (2004) Submerged or non-submerged healing of endosseous implants to be used in the rehabilitation of partially dentate patients. *Journal of Clinical Periodontology* **31**, 299–308. doi:10.1111/j.1600-051X.2004.00527.x.

Cha, J. Y., Pereira, M. D., Smith, A. A., Houschyar, K. S., Yin, X., Mouraret, S., Brunski, J. B. & Helms, J. A. (2015) Multiscale analyses of the bone-implant interface. *Journal of Dental Research* **94**, 482–490. doi:10.1177/0022034514566029.

Chen, H. M., Pahl, H. L., Scheibe, R. J., Zhang, D. E. & Tenen, D. G. (1993) The Sp1 transcription factor binds the CD11b promoter specifically in myeloid cells in vivo and is essential for myeloid-specific promoter activity. *Journal of Biological Chemistry* **268**, 8230–8239.

Coleman, D. L., King, R. N. & Andrade, J. D. (1974) The foreign body reaction: a chronic inflammatory response. *Journal of Biomedical Materials Research* **8**, 199–211. doi:10.1002/jbm.820080503.

Dhamdhere, G. R., Fang, M. Y., Jiang, J., Lee, K., Cheng, D., Olveda, R. C., Liu, B., Mulligan, K. A., Carlson, J. C., Ransom, R. C., Weis, W. I. & Helms, J. A. (2014) Drugging a stem cell compartment using Wnt3a protein as a therapeutic. *PLoS ONE* **9**, e83650. doi:10.1371/journal.pone.0083650.

Elmengaard, B., Bechtold, J. E. & Soballe, K. (2005) In vivo effects of RGD-coated titanium implants inserted in two bone-gap models. *Journal of Biomedical Materials Research. Part A* **75**, 249–255. doi:10.1002/jbm.a.30301.

Esposito, M., Thomsen, P., Ericson, L. E., Sennerby, L. & Lekholm, U. (2000) Histopathologic observations on late oral implant failures. *Clinical Implant Dentistry and Related Research* **2**, 18–32.

Fulciniti, M., Tassone, P., Hideshima, T., Vallet, S., Nanjappa, P., Ettenberg, S. A., Shen, Z., Patel, N., Tai, Y. T., Chauhan, D., Mitsiades, C., Prabhala, R., Raje, N., Anderson, K. C., Stover, D. R. & Munshi, N. C. (2009) Anti-DKK1 mAb (BHQ880) as a potential therapeutic agent for multiple myeloma. *Blood* **114**, 371–379. doi:10.1182/blood-2008-11-191577.

Grandi, T., Guazzi, P., Samarani, R. & Grandi, G. (2013) Clinical outcome and bone healing of implants placed with high insertion torque: 12-month results from a multicenter controlled cohort study. *International Journal of Oral and Maxillofacial Surgery* **42**, 516–520. doi:10.1016/j.ijom.2012.10.013.

Hughes, F. J., Turner, W., Belibasakis, G. & Martuscelli, G. (2006) Effects of growth factors and cytokines on osteoblast differentiation. *Periodontology 2000* **41**, 48–72. doi:10.1111/j.1600-0757.2006.00161.x.

Javed, F. & Romanos, G. E. (2010) The role of primary stability for successful immediate loading of dental implants. A literature review.

Journal of Dentistry **38**, 612–620. doi:10.1016/j.jdent.2010.05.013.

Jimbo, R., Tovar, N., Yoo, D. Y., Janal, M. N., Anchieta, R. B. & Coelho, P. G. (2014) The effect of different surgical drilling procedures on full laser-etched microgrooves surface-treated implants: an experimental study in sheep. *Clinical Oral Implants Research* **25**, 1072–1077. doi:10.1111/clr.12216.

Jing, W., Smith, A. A., Liu, B., Li, J., Hunter, D. J., Dhamdhere, G., Salmon, B., Jiang, J., Cheng, D., Johnson, C. A., Chen, S., Lee, K., Singh, G. & Helms, J. A. (2015) Reengineering autologous bone grafts with the stem cell activator WNT3A. *Biomaterials* **47**, 29–40. doi:10.1016/j.biomaterials.2014.12.014.

Kastellorizios, M., Tipnis, N. & Burgess, D. J. (2015) Foreign body reaction to subcutaneous implants. *Advances in Experimental Medicine and Biology* **865**, 93–108. doi:10.1007/978-3-319-18603-0_6.

Kretzschmar, K. & Watt, F. M. (2012) Lineage tracing. *Cell* **148**, 33–45. doi:10.1016/j.cell.2012.01.002.

Leucht, P., Jiang, J., Cheng, D., Liu, B., Dhamdhere, G., Fang, M. Y., Monica, S. D., Urena, J. J., Cole, W., Smith, L. R., Castillo, A. B., Longaker, M. T. & Helms, J. A. (2013) Wnt3a reestablishes osteogenic capacity to bone grafts from aged animals. *Journal of Bone and Joint Surgery. American Volume* **95**, 1278–1288. doi:10.2106/JBJS.L.01502.

Leucht, P., Kim, J. B., Amasha, R., James, A. W., Girod, S. & Helms, J. A. (2008) Embryonic origin and Hox status determine progenitor cell fate during adult bone regeneration. *Development* **135**, 2845–2854. doi:10.1242/dev.023788.

Lim, W. H., Liu, B., Cheng, D., Hunter, D. J., Zhong, Z., Ramos, D. M., Williams, B. O., Sharpe, P. T., Bardet, C., Mah, S. J. & Helms, J. A. (2014) Wnt signaling regulates pulp volume and dentin thickness. *Journal of Bone and Mineral Research* **29**, 892–901. doi:10.1002/jbmr.2088.

Lioubavina-Hack, N., Lang, N. P. & Karring, T. (2006) Significance of primary stability for osseointegration of dental implants. *Clinical Oral Implants Research* **17**, 244–250. doi:10.1111/j.1600-0501.2005.01201.x.

Minear, S., Leucht, P., Jiang, J., Liu, B., Zeng, A., Fuerer, C., Nusse, R. & Helms, J. A. (2010) Wnt proteins promote bone regeneration. *Science Translational Medicine* **2**, 29ra30. doi:10.1126/scitranslmed.3000231.

Morrell, N. T., Leucht, P., Zhao, L., Kim, J. B., ten Berge, D., Ponnusamy, K., Carre, A. L., Dudek, H., Zachlederova, M., McElhaney, M., Brunton, S., Gunzner, J., Callow, M., Polakis, P., Costa, M., Zhang, X. M., Helms, J. A. & Nusse, R. (2008) Liposomal packaging generates Wnt protein with in vivo biological activity. *PLoS ONE* **3**, e2930.

Mouraret, S., Hunter, D. J., Bardet, C., Brunski, J. B., Bouchard, P. & Helms, J. A. (2013) A pre-clinical murine model of oral implant osseointegration. *Bone* **58**, 177–184. doi:10.1016/j.bone.2013.07.021.

Mouraret, S., Hunter, D. J., Bardet, C., Brunski, J. B., Bouchard, P. & Helms, J. A. (2014a) A pre-clinical murine model of oral implant osseointegration. *Bone* **58**, 177–184. doi:10.1016/j.bone.2013.07.021.

Mouraret, S., Hunter, D. J., Bardet, C., Popelut, A., Brunski, J. B., Chaussain, C., Bouchard, P. & Helms, J. A. (2014b) Improving oral implant osseointegration in a murine model via Wnt signal amplification. *Journal of Clinical Periodontology* **41**, 172–180. doi:10.1111/jcpe.12187.

Movat, H. Z. (1955) Demonstration of all connective tissue elements in a single section; pentachrome stains. *A.M.A. Archives of Pathology* **60**, 289–295.

Nakashima, K., Zhou, X., Kunkel, G., Zhang, Z., Deng, J. M., Behringer, R. R. & de Crombrugghe, B. (2002) The novel zinc finger-containing transcription factor osterix is required for osteoblast differentiation and bone formation. *Cell* **108**, 17–29.

O'Sullivan, D., Sennerby, L., Jagger, D. & Meredith, N. (2004) A comparison of two methods of enhancing implant primary stability. *Clinical Implant Dentistry and Related Research* **6**, 48–57.

Pape, H. C., Evans, A. & Kobbe, P. (2010) Autologous bone graft: properties and techniques. *Journal of Orthopaedic Trauma* **24**(Suppl. 1), S36–S40. doi:10.1097/BOT.0b013e3181cec4a1.

Pazianas, M. & Abrahamsen, B. (2011) Safety of bisphosphonates. *Bone* **49**, 103–110. doi:10.1016/j.bone.2011.01.003.

Popelut, A., Rooker, S. M., Leucht, P., Medio, M., Brunski, J. B. & Helms, J. A. (2010) The acceleration of implant osseointegration by liposomal Wnt3a. *Biomaterials* **31**, 9173–9181. doi:10.1016/j.biomaterials.2010.08.045.

Recker, R. R., Benson, C. T., Matsumoto, T., Bolognese, M. A., Robins, D. A., Alam, J., Chiang, A. Y., Hu, L., Krege, J. H., Sowa, H., Mitlak, B. H. & Myers, S. L. (2015) A randomized, double-blind phase 2 clinical trial of blosozumab, a sclerostin antibody, in postmenopausal women with low bone mineral density. *Journal of Bone and Mineral Research* **30**, 216–224. doi:10.1002/jbmr.2351.

Rolfe, B., Mooney, J., Zhang, B., Jahnke, S., Le, S.-J., Cahau, Y.-Q., Huang, Q., Wang, H., Campbell, G. R. & Campbell, J. (2011) The Fibrotic Response to Implanted Biomaterials: Implications for Tissue Engineering.

Sela, J., Applebaum, J. & Uretzky, G. (1986) Osteogenesis induced by bone matrix is inhibited by inflammation. *Biomaterials, Medical Devices, and Artificial Organs* **14**, 227–237.

Smith, A. J. (2015) New horizons in therapeutic antibody discovery: opportunities and challenges versus small-molecule therapeutics. *Journal of Biomolecular Screening* **20**, 437–453. doi:10.1177/1087057114562544.

Soballe, K., Hansen, E. S., Brockstedt-Rasmussen, H., Pedersen, C. M. & Bunger, C. (1992) Bone graft incorporation around titanium-alloy- and hydroxyapatite-coated implants in dogs. *Clinical Orthopaedics and Related Research* **274**, 282–293.

Tonetti, M. S. & Schmid, J. (1994) Pathogenesis of implant failures. *Periodontology 2000* **4**, 127–138.

Virdi, A. S., Irish, J., Sena, K., Liu, M., Ke, H. Z., McNulty, M. A. & Sumner, D. R. (2015) Sclerostin antibody treatment improves implant fixation in a model of severe osteoporosis. *Journal of Bone and Joint Surgery. American Volume* **97**, 133–140. doi:10.2106/JBJS.N.00654.

Whyte, J. L., Smith, A. A., Liu, B., Manzano, W. R., Evans, N. D., Dhamdhere, G. R., Fang, M. Y., Chang, H. Y., Oro, A. E. & Helms, J. A. (2013) Augmenting endogenous Wnt signaling improves skin wound healing. *PLoS ONE* **8**, e76883. doi:10.1371/journal.pone.0076883.

Yaccoby, S., Ling, W., Zhan, F., Walker, R., Barlogie, B. & Shaughnessy, J. D. Jr (2007) Antibody-based inhibition of DKK1 suppresses tumor-induced bone resorption and multiple myeloma growth in vivo. *Blood* **109**, 2106–2111. doi:10.1182/blood-2006-09-047712.

Yin, X., Li, J., Salmon, B., Huang, L., Lim, W. H., Liu, B., Hunter, D. J., Ransom, R. C., Singh, G., Gillette, M., Zou, S. & Helms, J. A. (2015) Wnt signaling and its contribution to craniofacial tissue homeostasis. *Journal of Dental Research* **94**(11), 1487–1494. doi:10.1177/0022034515599772.

Zhao, L., Rooker, S. M., Morrell, N., Leucht, P., Simanovskii, D. & Helms, J. A. (2009) Controlling the in vivo activity of Wnt liposomes. *Methods in Enzymology* **465**, 331–347.

Supporting Information

Additional Supporting Information may be found in the online version of this article:

Fig. S1. Histology and FE model of the peri-implant interfaces around tight-fit implants. Representative tissue sections stained with Movat's pentachrome, aniline blue, and picrosirius red on (A-C) PID7, (D-F) 14 and (G-I) 21. (J) Principal compressive strain and principal tensile strain in the tight-fit bone-implant interface. Abbreviations: b, bone; FEA, finite element analyses; im, implant; PID, post-implant day; WT, wild-type. Scale bar = 50 μm for all panels.

Fig. S2. Collagen type I expression wanes around gap-type implants. (A) Representative tissue section immunostained with collagen type I on PID7 ($N = 12$), (B) 14 ($N = 12$) and (C) 21 ($N = 12$). Abbreviations: b, bone; Col I, collagen type I; fe, fibrous envelope; im, implant; PID, post-implant day; WT, wild-type. Scale bar = 50 μm for all panels.

Fig. S3. L-WNT3A treatment permits bone remodelling (A) Representative sagittal tissue sections stained with TRAP to detect osteoclast activity after L-PBS ($N = 12$) and (B) L-WNT3A ($N = 12$) injections. Abbreviations: b, bone; fe, fibrous envelope; im, implant; PID, post-implant day; WT, wild-type. Scale bar = 50 μm for all panels.

Table S1. Implants subjected to lateral stiffness testing

Table S2. Experimental numbers by type of implant interface

Table S3. Experimental numbers by genotype and treatment group

Table S4. Parameters of the implant interface

Table S5. Parameters used in finite element analyses

Address:
Jill A. Helms
Division of Plastic and Reconstructive Surgery
Department of Surgery
Stanford School of Medicine
Room GK207, 257 Campus Dr.
Stanford, CA 94305
USA
E-mail: jhelms@stanford.edu

Clinical Relevance

Scientific rationale for the study: Failed implants undergo fibrous encapsulation. We tested whether local delivery of a potent bone-inducing WNT protein was sufficient to convert a fibrous tissue capsule into peri-implant bone.

Principal findings: Using an oral implant model where primary stability is lacking, we find that local injection of a WNT protein therapeutic induces peri-implant bone formation, leading to significantly more bone in contact with the implant.

Practical implications: A WNT-based biological approach has the potential to salvage implants in suboptimal clinical situations where anatomy or disease has compromised the implant bed.